AD-A192 759 COMPACT HIGH ORDER SCHEMES FOR THE EULER EQUATIONS(U) 1/1
INSTITUTE FOR COMPUTER APPLICATIONS IN SCIENCE AND
ENGINEERIN.. S ABARBANEL ET AL. FEB 88 ICASE-88-13
UNCLASSIFIED NASA-CR-181625 NAS1-18107 F/G 12/1 NL

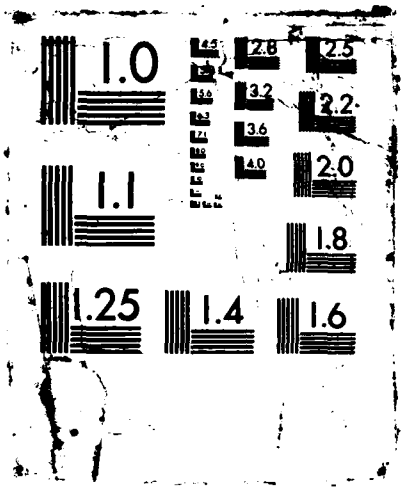
1.0
1.1
1.25
1.4
1.6
1.8
2.0
2.2
2.5
2.8
3.2
3.6
4.0
4.5

NASA Contractor Report 181625
ICASE Report No. 88-13

ICASE

COMPACT HIGH ORDER SCHEMES FOR THE EULER EQUATIONS

Saul Abarbanel
Ajay Kumar

Contract No. NAS1-18107
February 1988

INSTITUTE FOR COMPUTER APPLICATIONS IN SCIENCE AND ENGINEERING
NASA Langley Research Center, Hampton, Virginia 23665

Operated by the Universities Space Research Association

National Aeronautics and Space Administration
Langley Research Center
Hampton, Virginia 23665

COMPACT HIGH ORDER SCHEMES FOR THE EULER EQUATIONS

Saul Abarbanel
Tel-Aviv University

and

Ajay Kumar
NASA Langley Research Center

ABSTRACT

An implicit approximate factorization (AF) algorithm is constructed which has the following characteristics.

- In 2-D: The scheme is unconditionally stable, has a 3×3 stencil and at steady state has a fourth order spatial accuracy. The temporal evolution is time accurate either to 1st or 2nd order through choice of parameter.
- In 3-D: The scheme has almost the same properties as in 2-D except that it is now only conditionally stable, with the stability condition (the CFL number) being dependent on the "cell aspect ratios," $\Delta y/\Delta x$ and $\Delta z/\Delta x$. The stencil is still compact and fourth order accuracy at steady state is maintained.

Numerical experiments on a 2-D shock-reflection problem show the expected improvement over lower order schemes, not only in accuracy (measured by the L_2 error) but also in the dispersion.

It is also shown how the same technique is immediately extendable to Runge-Kutta type schemes resulting in improved stability in addition to the enhanced accuracy. [1]

[1]This research was supported by the National Aeronautics and Space Administration under NASA Contract No. NAS1-18107 while the first author was in residence at the Institute for Computer Applications in Science and Engineering (ICASE), NASA Langley Research Center, Hampton, VA 23665. Partial support was also provided under USAF Grant No. AFOSR-87-0218.

1 INTRODUCTION

It can be shown [1] that numerical approximations to the linearized Euler equations of gas dynamics give rise to dispersive errors which in the 2-D supersonic case depend on a similarity parameter $\kappa = (\Delta y/\Delta x)\sqrt{M_\infty^2 - 1}$ (under the assumption $v \ll u$ everywhere, where u and v are the x and y components of the velocity vector). The difference between the dispersion relations of any numerical algorithm and that of the original partial differential equations can be plotted as curves in the Fourier plane with κ as a parameter.

In particular the results in [1] indicate that for central-difference schemes, the dispersive error are contributed mostly by the third power of the errors in the Fourier variables θ and ϕ. It is, therefore, natural to think of fourth order spatially accurate algorithms as having better dispersive properties. By utilizing the structure of the Euler equations one can obtain, on a cartesian grid, a fourth order approximation which instead of using a 5×5 stencil (and $5 \times 5 \times 5$ in 3-D) relies on a compact support of 3×3 (and $3 \times 3 \times 3$ in 3-D). The advantages of the combination of fourth order accuracy together with compact support are quite obvious in terms of total computer work and memory.

In Section 2, we describe the construction of an approximate factorization (AF) central difference scheme and examine its theoretical (linear) stability properties. In Section 3, we derive the corresponding 4-step Runge-Kutta scheme and show how the Jameson-Schmidt-Turkel algorithms [2] may be easily modified to that form which has, in addition to the higher accuracy, markedly enhanced stability limits. In Section 4, we describe some numerical experiments using the AF-version. Section 5 summarizes our findings.

2 DERIVATION OF THE APPROXIMATE-FACTORIZATION SCHEME

2.1 The Two-Dimensional Case

Consider a general hyperbolic conservation law in 2-D:

$$\vec{u}_t + \vec{f}_x + \vec{g}_y = 0. \tag{1}$$

In the case of Euler equations, for example, the vectors $\vec{u}, \vec{f}\,(\vec{u}), \vec{g}\,(\vec{u})$ are given by

$$\vec{u} = \begin{pmatrix} \rho \\ \rho u \\ \rho v \\ E \end{pmatrix} \quad \vec{f} = \begin{pmatrix} \rho u \\ \rho u^2 + p \\ \rho uv \\ u(E+p) \end{pmatrix} \quad \vec{g} = \begin{pmatrix} \rho v \\ \rho vu \\ \rho v^2 + p \\ v(E+p) \end{pmatrix} \tag{2}$$

where ρ, u, v, E, and p are respectively the density, velocity components in the x and y directions, the total energy per unit volume and the pressure. In addition there is the equation of state relating algebraically (in the case of gas-dynamics) the internal energy to the pressure and density. One may also write (1) in non-conservation form as

$$\vec{u}_t + A\,\vec{u}_x + B\,\vec{u}_y = 0 \tag{3}$$

where A and B are the Jacobians of $\vec{f}$ and $\vec{g}$ with respect to $\vec{u}$.

Consider first a forward-time second order central finite difference approximation to (1)

$$\frac{u_{j,k}^{n+1} - u_{j,k}^{n}}{\Delta t} + \frac{f_{j+1,k}^{n} - f_{j-1,k}^{n}}{\Delta x} + \frac{g_{j,k+1}^{n} - g_{j,k-1}^{n}}{\Delta y} = 0 \tag{4}$$

where we have dropped the sup-arrow indicating a vector and used the conventional differencing notation

$$\vec{u_{j,k}} = u_{j,k}^{n} = u(j\Delta x, k\Delta y, n\Delta t). \tag{5}$$

We have a cartesian grid with nodes at $x = j\Delta x, y = k\Delta y$ and $t = n\Delta t$. We shall now introduce the usual shift operations notation:

$$\begin{aligned} D_t u &= u_{j,k}^{n+1} - u_{j,k}^{n} \\ \mu_x u &= \tfrac{1}{2}(u_{j+\frac{1}{2},k} + u_{j-\frac{1}{2},k}), \quad \mu_y = \tfrac{1}{2}(u_{j,k+\frac{1}{2}} + u_{j,k-\frac{1}{2}}) \\ \delta_x u &= u_{j+\frac{1}{2},k} - u_{j-\frac{1}{2},k}, \qquad \delta_y = u_{j,k+\frac{1}{2}} - u_{j,k-\frac{1}{2}}. \end{aligned} \tag{6}$$

Eq. (4) then may be written as:

$$D_t u = -\lambda \mu_x \delta_x f - \frac{\delta}{I\!R} \mu_y \delta_y g \tag{7}$$

where $\lambda = \Delta t/\Delta x$ and $I\!R = \Delta y/\Delta x$. If we take a Taylor series expansion about the grid point $(x, y, t) = (j\Delta x, k\Delta y, n\Delta t)$, we can construct the modified equation corresponding to (7):

$$u_t + \frac{\Delta t}{2} u_{tt} + \cdots = -\left[f_x + \frac{\Delta x^2}{3!} f_{xxx} + \cdots\right] - \left[g_y + \frac{\Delta y^2}{3!} g_{yyy} + \cdots\right]$$

or

$$u_t + f_x + g_y = -\left[\frac{\Delta t}{2} u_{tt} + \frac{\Delta x^2}{3!} f_{xxx} + \frac{\Delta y^2}{3!} g_{yyy}\right]. \tag{8}$$

Thus if we want to approximate (1) to a higher than second order (and in particular to fourth order in space–see comment in Introduction concerning dispersive errors) we must modify (7) by subtracting out the terms on the right hand side of (8). At this point we realize that using a straightforward approach to approximating f_{xxx} and g_{yyy} will lead to bigger stencils. However, using the original partial differential equation, (1), we have

$$f_{xxx} = -u_{txx} - g_{yxx} \tag{9}$$

and similarly

$$g_{yyy} = -u_{tyy} - f_{xyy}. \tag{10}$$

Since f_{xxx} and g_{yyy} need be approximated only to second order (because of their coefficients, $\Delta x^2/3$ and $\Delta y^2/3$) the required stencil for the terms on the right hand side is only 3×3. (This observation was previously made, in another context by Jones, et al. [3].) So, replacing f_{xxx} and g_{yyy} in (8) by $-\delta_x^2 D_t u/\Delta x^2 \Delta t - \delta_x^2 \mu_y \delta_y g/\Delta x^2 \Delta y$ and $-\delta_y^2 D_t u/\Delta y^2 \Delta t - \delta y^2 \mu_x \delta_x f/\Delta y^2 \Delta x$, respectively; and also replacing u_{tt} by $D_t u_t/\Delta t \to D_t(-f_x - g_y)/\Delta t \to -D_t\left[(\mu_x \delta_x f/\Delta x) + (\mu_y \delta_y g/\Delta y)\right]$ we obtain the following approximation to (1) which is spatially fourth order accurate and temporally second order accurate:

$$D_t\left[u + \frac{\Delta t}{2}\left(\frac{\mu_x \delta_x}{\Delta x} f + \frac{\mu y \delta y}{\Delta y} g\right) + \frac{\Delta x^2}{3!}\frac{\delta x^2}{\Delta x^2} f + \frac{\Delta y^2}{3!}\frac{\delta y^2}{\Delta y^2} g\right]$$

$$= -\lambda\mu_x\delta_x f - \frac{\lambda}{3!}\Delta x^3 \frac{\mu_y\delta_y\delta_x^2}{\Delta y\Delta x^2} g - \frac{\lambda}{I\!R}\mu_y\delta_y g - \frac{\lambda}{3!I\!R}\Delta y^3 \frac{\mu_x\delta_x\delta_y^2}{\Delta x\Delta y^2} f.$$

Using (3) and the definition of D_t we rearrange the above into the delta form

$$\left[I + \frac{\lambda}{2}\left(A\mu_x\delta_x + \frac{B}{I\!R}\mu_y\delta_y\right) + \frac{1}{3!}\left(A\delta_x^2 + B\delta_y^2\right)\right]\left(u_{j,k}^{n+1} - u_{j,k}^n\right)$$

$$= -\lambda\mu_x\delta_x\left(I + \frac{1}{3!}\delta_y^2\right) f_{j,k}^n - \frac{\lambda\mu_y\delta_y}{I\!R}\left(I + \frac{1}{3!}\delta_x^2\right) g_{j,k}^n \tag{11}$$

where I is the identity matrix. This is an implicit unfactored scheme. Since we are interested in marching to steady state we approximate-factor the left hand side to obtain:

$$\left(I + \frac{1}{3!}A\delta_x^2 + \frac{\sigma}{2}\lambda A\mu_x\delta_x\right)\left(I + \frac{1}{3!}B\delta_y^2 + \frac{\sigma}{2}\lambda\frac{B}{I\!R}\mu_y\delta y\right)\left(u_{j,k}^{n+1} - u_{j,k}^n\right)$$

$$= -\lambda\left\{\mu_x\delta_x\left(I + \frac{1}{3!}\delta_y^2\right) f_{j,k}^n + \frac{1}{I\!R}\mu_y\delta_y\left(I + \frac{1}{3!}\delta_x^2\right) g_{j,k}^n\right\}. \tag{12}$$

We introduced into (12) the parameter σ. If $\sigma = 1$ then we retain the temporal second order accuracy while $\sigma = 2$ gives first order in time. Note that (12) involves the inversion of block-tridiagonal matrices. The right hand side represents the steady state operator to fourth-order. The whole scheme involves only a 3 stencil.

2.2 The 3-D Case

The starting point, corresponding to (1) is

$$\vec{u_t} + \vec{f_x} + \vec{g_y} + \vec{h_z} = 0. \tag{13}$$

Following the same steps as in the 2-D case, we get the modified equation

$$u_t + f_x + g_y + h_z = -\left[\frac{\Delta t}{2}u_{tt} + \frac{\Delta x^2}{3!}f_{xxx} + \frac{\Delta y^2}{3!}g_{yyy} + \frac{\Delta z^2}{3!}h_{zzz}\right] \tag{14}$$

where using (13), we have

$$f_{xxx} = -u_{txx} - g_{yxx} - h_{xxx} \tag{15}$$

$$g_{yyy} = -u_{tyy} - h_{zyy} - f_{xyy} \tag{16}$$

$$h_{zzz} = -u_{tzz} - f_{xzz} - g_{yzz}. \tag{17}$$

Repeating all the steps leading to (12) we obtain its three dimensional analog:

$$\left(I + \frac{1}{3!}A\delta_x^2 + \frac{\sigma}{2}\lambda A\mu_x\delta_x\right)\left(I + \frac{1}{3!}B\delta_y^2 + \frac{\sigma}{2}\lambda\frac{B}{I\!R}\mu_y\delta_y\right)\left(I + \frac{1}{3!}C\delta_z^2 + \frac{\sigma}{2}\lambda\frac{C}{Q}\mu_z\delta_z\right)\left(u_{j,k,\ell}^{n+1} - u_{j,k,\ell}^n\right) =$$

$$= -\lambda\left[\mu_x\delta_x\left(I + \frac{1}{3!}\delta_y^2 + \frac{1}{3!}\delta_z^2\right) f_{j,k,\ell}^n + \mu_y\delta_y\left(I + \frac{1}{3!}\delta_z^2 + \frac{1}{3!}\delta_z^2\right) g_{j,k,\ell}^n + \mu_z\delta_z\left(I + \frac{1}{3!}\delta_z^2 + \frac{1}{3!}\delta_y^2\right) h_{j,k,l}^n\right]. \tag{18}$$

In (18) the matrix C is the Jacobian $\partial\ \vec{h}\ /\partial\ \vec{u}$ and the shift operators μ_z, δ_z are defined in a manner analogous to (6). Q is the cell aspect ratio in the z direction, $Q = \Delta z/\Delta x$.

2.3 Stability Analysis for the 2-D Case

We consider the linearized (i.e., frozen coefficients) version of (12). We carry out a Von-Neumann analysis in the usual manner by casting (12) in Fourier space. A typical Fourier component of $u^n_{j,k}$ is given by

$$u^n_{j,k} \rightarrow \hat{u}^n e^{ij\phi} e^{ik\theta} \tag{19}$$

where

$$\phi = \ell\Delta x, \quad \theta = m\Delta y \tag{20}$$

with

$$-\pi < \phi, \theta < \pi \quad and \quad -\infty < \ell, m < \infty. \tag{21}$$

The mapping of the various shift operations is as follows:

$$\delta_x u^n_{j,k} \rightarrow 2isin\frac{\phi}{2} \triangleq 2i\xi, \qquad \delta_y u^n_{j,k} \rightarrow 2isin\frac{\theta}{2} \triangleq 2i\eta \tag{22}$$

$$\mu_x u^n_{j,k} \rightarrow cos\frac{\phi}{2} = \sqrt{1-\xi^2}, \quad \mu_y u^n_{j,k} \rightarrow cos\frac{\theta}{2} = \sqrt{1-\eta^2} \tag{23}$$

$$\delta_x^2 u^n_{j,k} \rightarrow -4sin^2\frac{\phi}{2} = -4\xi^2, \quad \delta_y^2 u^n_{j,k} \rightarrow -4sin^2\frac{\theta}{2} = -4\eta^2 \tag{24}$$

and so,

$$\mu_x\delta_x u^n_{j,k} \rightarrow 2i\xi\sqrt{1-\xi^2}, \quad \mu_y\delta_y u^n_{j,k} \rightarrow 2i\eta\sqrt{1-\eta^2}. \tag{25}$$

We also define the amplification matrix G by $\hat{u}^{n+1} = G\hat{u}^n$. With these notations, the frozen coefficient version of (12) is mapped into the Fourier space as follows:

$$\left(I - \frac{2}{3}A\xi^2 + i\sigma\lambda A\xi\sqrt{1-\xi^2}\right)\left(I - \frac{2}{3}B\eta^2 + i\sigma\frac{\lambda B}{I\!R}\eta\sqrt{1-\eta^2}\right)(G-I)$$

$$= -2i\lambda\left[A\xi\sqrt{1-\xi^2}\left(I - \frac{2}{3}\eta^2\right) + \frac{B}{I\!R}\eta\sqrt{1-\eta^2}\left(I - \frac{2}{3}\xi^2\right)\right]. \tag{26}$$

In the general case the matrices A and B do not commute, thus rendering the analysis of (26) almost intractable. It is instructive, however, to consider the scalar case. Since the aspect ratio $I\!R = \Delta y/\Delta x$ is arbitrary, and since the original partial differential equation (1), in the scalar linear case, could be transformed to the wave equation

$$u_{\bar{t}} + u_{\bar{t}} + u_{\bar{y}} = 0$$

with $\bar{t} = At, \bar{x} = x$ and $\bar{y} = Ay/B$, we can without loss of generality (in this special linear scalar case) rewrite (26) as:

$$\left(1 - \frac{2}{3}\xi^2 + i\sigma\lambda\xi\sqrt{1-\xi^2}\right)\left(1 - \frac{2}{3}\eta^2 + \frac{i\sigma\lambda\eta}{I\!R}\sqrt{1-\eta^2}\right)(G-1)$$

$$= -2i\lambda\left[\xi\sqrt{1-\xi^2}\left(1 - \frac{2}{3}\eta^2\right) + \frac{1}{I\!R}\eta\sqrt{1-\eta^2}\left(1 - \frac{2}{3}\xi^2\right)\right]. \tag{27}$$

Equation (27) can be rearranged to solve for the amplification factor G :

$$G = \frac{a + i(\frac{\sigma}{2} - 1)b}{a + i\frac{\sigma}{2}b} \tag{28}$$

where

$$a = 1 - \frac{2}{3}\xi^2 - \frac{2}{3}\eta^2 + \frac{4}{9}\xi^2\eta^2 - \frac{1}{I\!R}\sigma^2\lambda^2\xi\eta\sqrt{1-\xi^2}\sqrt{1-\eta^2} \tag{29}$$

and b is the Fourier map of the steady-state operator, i.e.:

$$b = 2\left[\lambda\xi\sqrt{1-\xi^2}(1-\frac{2}{3}\eta^2) + \frac{\lambda\eta}{I\!R}\sqrt{1-\eta^2}(1-\frac{2}{3}\xi^2)\right]. \tag{30}$$

We see immediately from (28) that for $\sigma = 1$ (i.e., the case of second order temporal accuracy) we have a Crank-Nicholson type scheme with $\|G\| = 1$. For $\sigma > 1$ (i.e., first order accuracy in time), we have $\|G\| < 1$. We have thus demonstrated the unconditional stability of (27) for all values of the cell aspect ratio.

2.4 Stability for the 3-D Case

The three dimensional analog to (27) is

$$(1 - \frac{2}{3}\xi^2 + i\sigma\lambda\xi\sqrt{1-\xi^2})(1 - \frac{2}{3}\eta^2 + i\sigma\frac{\lambda}{I\!R}\eta\sqrt{1-\eta^2})(1 - \frac{2}{3}\varsigma^2 + i\sigma\frac{\lambda}{Q}\varsigma\sqrt{1-\varsigma^2})(G-1) =$$

$$= -2i\lambda\left[\xi\sqrt{1-\xi^2}(1-\frac{2}{3}\eta^2-\frac{2}{3}\varsigma^2) + \frac{1}{I\!R}\eta\sqrt{1-\eta^2}(1-\frac{2}{3}\varsigma^2-\frac{2}{3}\xi^2) + \frac{1}{Q}\varsigma\sqrt{1-\varsigma^2}(1-\frac{2}{3}\xi^2-\frac{2}{3}\eta^2)\right] \tag{31}$$

where ς is the Fourier dual variable defined analogously to ξ and η.

The stability of three dimensional amplification factor G, as defined by (31), is difficult to analyze and we resorted to numerical evaluations of $|G|^2$, using up to 8×10^6 Fourier modes. The numerical study of (31) was carried out on the Cray 2. We found that as in the case of forward Euler approximate factorization second order scheme [4], the amplification factor was conditionally stable. For example for $I\!R = Q = 1$, the stability limit is $\lambda \leq .43$. These stability properties are obtained with the aid of artificial viscosity (AV) term which is of sixth order but still resides on the compact stencil. The AV term is added to the right hand side (explicit term) of (18) and is of the form

$$\mu_{av}\lambda\frac{1}{6!}\delta_x^2\delta_y^2\delta_z^2 \tag{32}$$

where μ_{av} is of order unity. We found $1.5 < \mu_{av} < 2$ to be most efficacious. Without the artificial viscosity term, the allowed value of λ is about one order of magnitude less (e.g., for $R = Q = 1, \lambda$ without using AV is about .035).

3 COMPACT FOUR STEP FOURTH ORDER RUNGE-KUTTA ALGORITHM

The basic four step explicit Runge-Kutta scheme, as proposed in [2], takes the form:

$$\begin{aligned} u^0 &= u^n \\ u^{(1)} &= u^{(n)} - \tfrac{1}{4}\Delta t R(u^{(0)}) \\ u^{(2)} &= u^{(n)} - \tfrac{1}{3}\Delta t R(u^{(1)}) \\ u^{(3)} &= u^{(n)} - \tfrac{1}{2}\Delta t R(u^{(2)}) \\ u^{(4)} &= u^{(n)} - \Delta t R(u^{(3)}) \\ u^{(n+1)} &= u^{(4)} \end{aligned} \tag{33}$$

where R is the finite difference (or finite volume) representation of the steady operator. For example, in the 2-D second order spatial accuracy case

$$R(u) = \frac{\mu_x \delta_x}{\Delta x} f + \frac{\mu_y \delta_y}{\Delta y} g \tag{34}$$

where f and g are the flux vectors encountered in section 2. If we want fourth order spatial accuracy, then it follows directly that the residual R is modified to read

$$R = \frac{\mu_x \delta_x}{\Delta x}(1 + \frac{1}{6}\delta_y^2) f + \frac{\mu_y \delta_y}{\Delta y}(1 + \frac{1}{6}\delta_x^2) g \tag{35}$$

and we still retain the compact support.

Similarly, in the <u>three dimensional</u> case we have

$$R = \frac{\mu_x \delta_x}{\Delta x}(1 + \frac{1}{6}\delta_y^2 + \frac{1}{6}\delta_z^2) f + \frac{\mu_y \delta_y}{\Delta y}(1 + \frac{1}{6}\delta_z^2 + \frac{1}{6}\delta_x^2) g + \frac{\mu_z \delta_z}{\Delta z}(1 + \frac{1}{6}\delta_z^2 + \frac{1}{6}\delta_y^2) h. \tag{36}$$

Thus (33), with R given either by (35) for the 2-D case or by (36) for the 3-D case, retains all the features of the second order scheme but gains us the fourth order accuracy. In addition one can easily verify by simple analysis that for a given cartesian grid and flow conditions the new fourth order formulation enhances the stability condition. In the 2-D case we have, using (35) rather than (34)

$$\frac{(\Delta t)_{(4)}}{(\Delta t)_{(2)}} \triangleq \frac{(\Delta t)_{4th\ order}}{(\Delta t)_{2nd\ order}} = 1.36. \tag{37}$$

In the 3-D case the gain is even more favorable,

$$\frac{(\Delta t)_4}{(\Delta t)_2} = 1.66. \tag{38}$$

Thus the algorithm efficiency gains are two fold. First, for a given acceptable error level the fourth order accuracy allows a coarser grid, i.e., fewer node points. Second, not only Δt is increased due to the larger cell size but in addition it gains due to (37) (or (38) in the 3-D case).

4 NUMERICAL RESULTS FOR 2-D CASE

The two-dimensional fourth order compact scheme is applied to a shock reflection problem sketched in Figure 1. It shows a 5° shock at Mach 1.95 reflecting from a flat plate. Results are presented both without any explicit artificial viscosity (AV) and with a fourth order AV term of the type $-\frac{\epsilon}{4!}(\delta_x^2\delta_y^2)$ added to the right hand side. Addition of this AV term reduced the accuracy of the compact scheme to third order (note that in 3-D the sixth order AV terms precludes this reduction in accuracy). Calculations are also made with a second order implicit Euler AF scheme without and with the preceding AV term. Figures 2a and 2b show the results of the compact scheme whereas Figures 3a and 3b show the corresponding results from the second order scheme. It is seen that for $\epsilon = 0$, both fourth and second order schemes produce very oscillatory results but with $\epsilon = 0.36$, the results from the compact scheme (Figure 2b) improve dramatically and, in fact, are much better than the corresponding results obtained from the second order scheme (Figure 3b). The shocks captured by the compact scheme are sharper and the convergence is also seen to improve.

Results from a study of grid aspect ratio effect on the compact scheme are also presented here in terms of the similarity parameter κ of reference 1. Three values of κ are considered, namely 1.67, 1.01, and 0.42. Figure 2b corresponds to $\kappa = 1.67$ and figures 4 and 5 correspond to $\kappa = 1.01$ and 0.42, respectively. In all these cases, ϵ is set equal to 0.36. It is clear from the figures displaying the effect of κ that the best results are obtained for κ near unity. In reference 1, a linear theory (e.g., for weak shock) predicts the same results. It is interesting that we find numerically that this is also the case in the present nonlinear problem.

SUMMARY

1. The steady state solution of the Euler equations of gas dynamics may be achieved to fourth order accuracy using a compact grid stencil of 3×3 and $3 \times 3 \times 3$ in the 2-D and 3-D cases respectively. We presented two examples of such algorithms: one implicit (Euler approximate factorizations scheme) and one explicit (Four-stage Runge-Kutta).

2. Numerical experiments were carried out for the 2-D shock reflection problem, using the implicit algorithm. Comparisons are made with a corresponding second order scheme. The results show that the compact higher order scheme offers marked improvement in both accuracy and convergence rate.

3. In connection with this work we would like to make the following remarks. It is known that the finite difference scheme cannot obtain high order accuracy for conservation-form equations computed on a non-uniform grid. This observation coupled with the ease of obtaining fourth order compact schemes even in 3-D for the Euler equations revives an old debate: Can one use uniform grid and apply conveniently boundary conditions to arbitrary shapes. The potential gain in reduced number of computational nodes and enhanced convergence rate appears large enough to study this question again.

References

[1] R. Shapiro, "Prediction of dispersive errors in numerical solutions of the Euler equations," submitted for presentation at the 2nd International Conference on Hyperbolic Problems, Aachen, West Germany, March 1988.

[2] A. Jameson, W. Schmidt, and E. Turkel, "Numerical solutions of the Euler equations by finite-volume methods using Runge-Kutta time-stepping schemes," AIAA Paper No. 81-1259, June 1981.

[3] D. J. Jones, J. C. South, and E. B. Klunker, "On the numerical solution of elliptic partial differential equations by the method of lines," J. Comp. Physics, Vol. 9, No. 3, June 1982, pp. 496-527.

[4] R. M. Beam and R. F. Warming, "An implicit factored scheme for the compressible Navier-Stokes equations," AIAA J., Vol. 16, 1978, pp. 393-401.

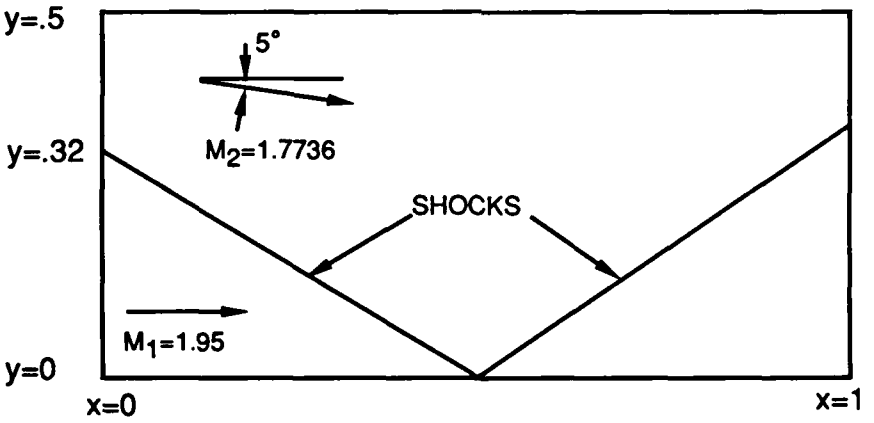

Figure 1: Shock reflection problem

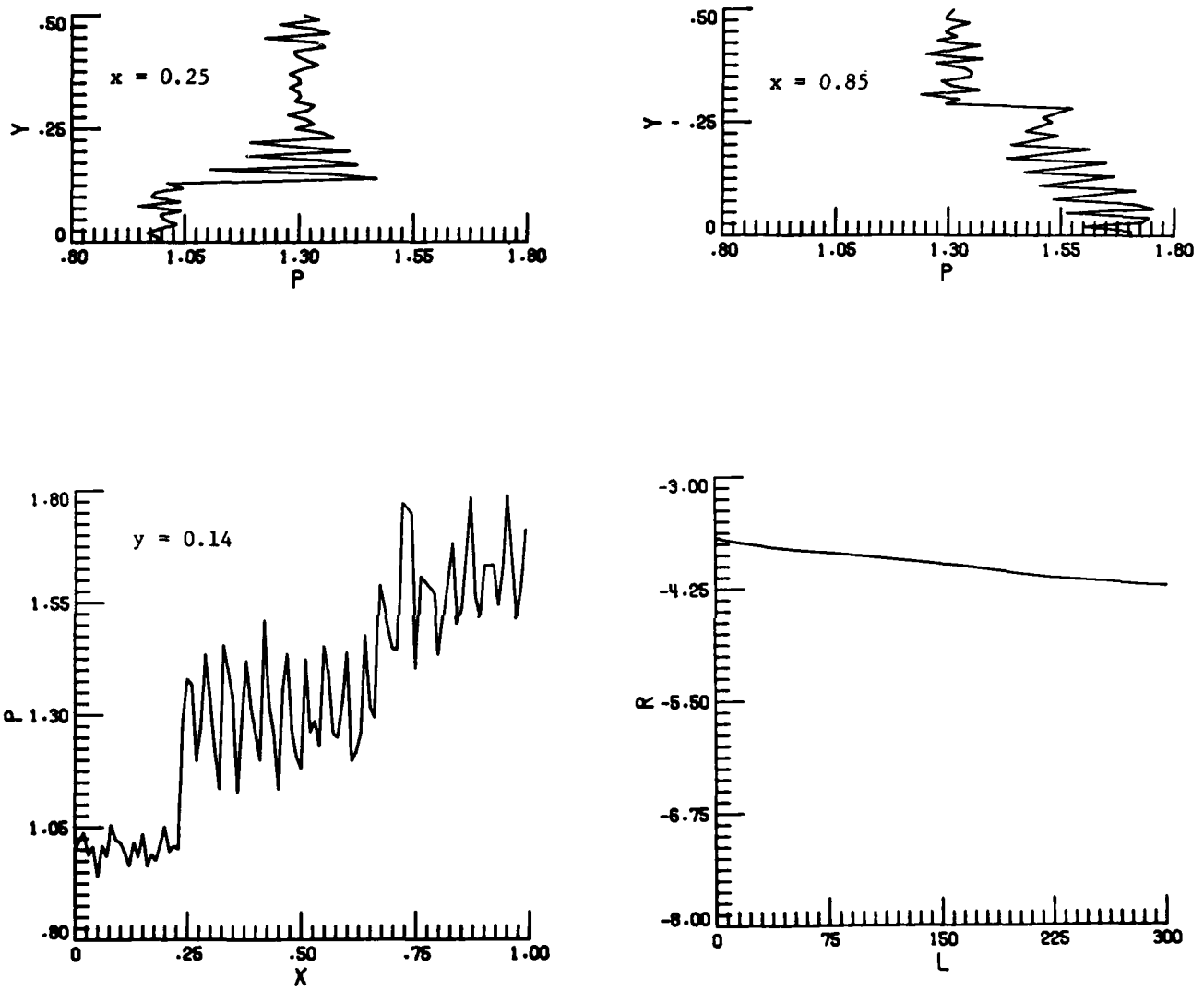

Figure 2a: Pressure distribution and residual plot for compact scheme ($\epsilon = 0, \kappa = 1.67$).

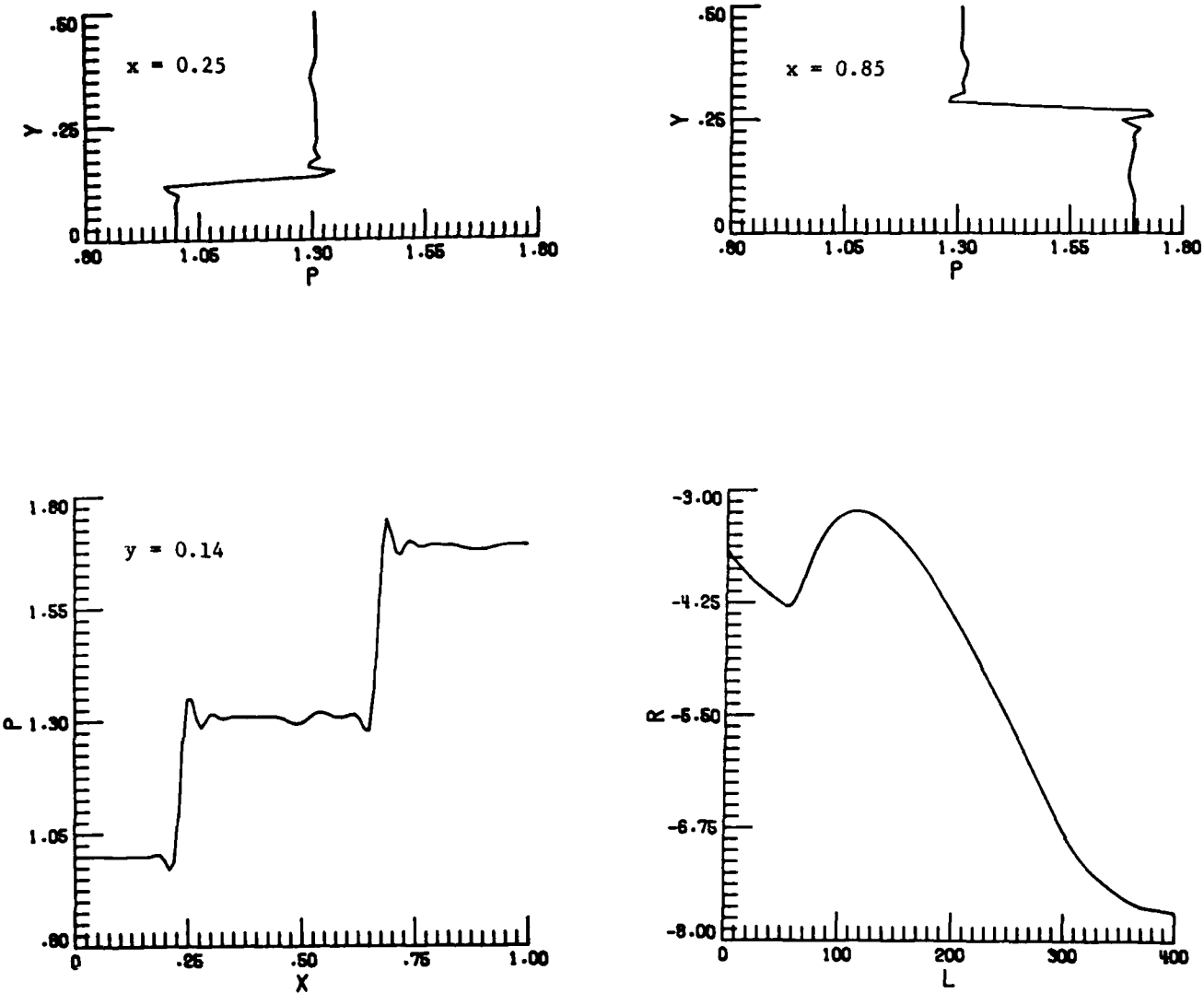

Figure 2b: Pressure distribution and residual plot for compact scheme ($\epsilon = 0.36, \kappa = 1.67$).

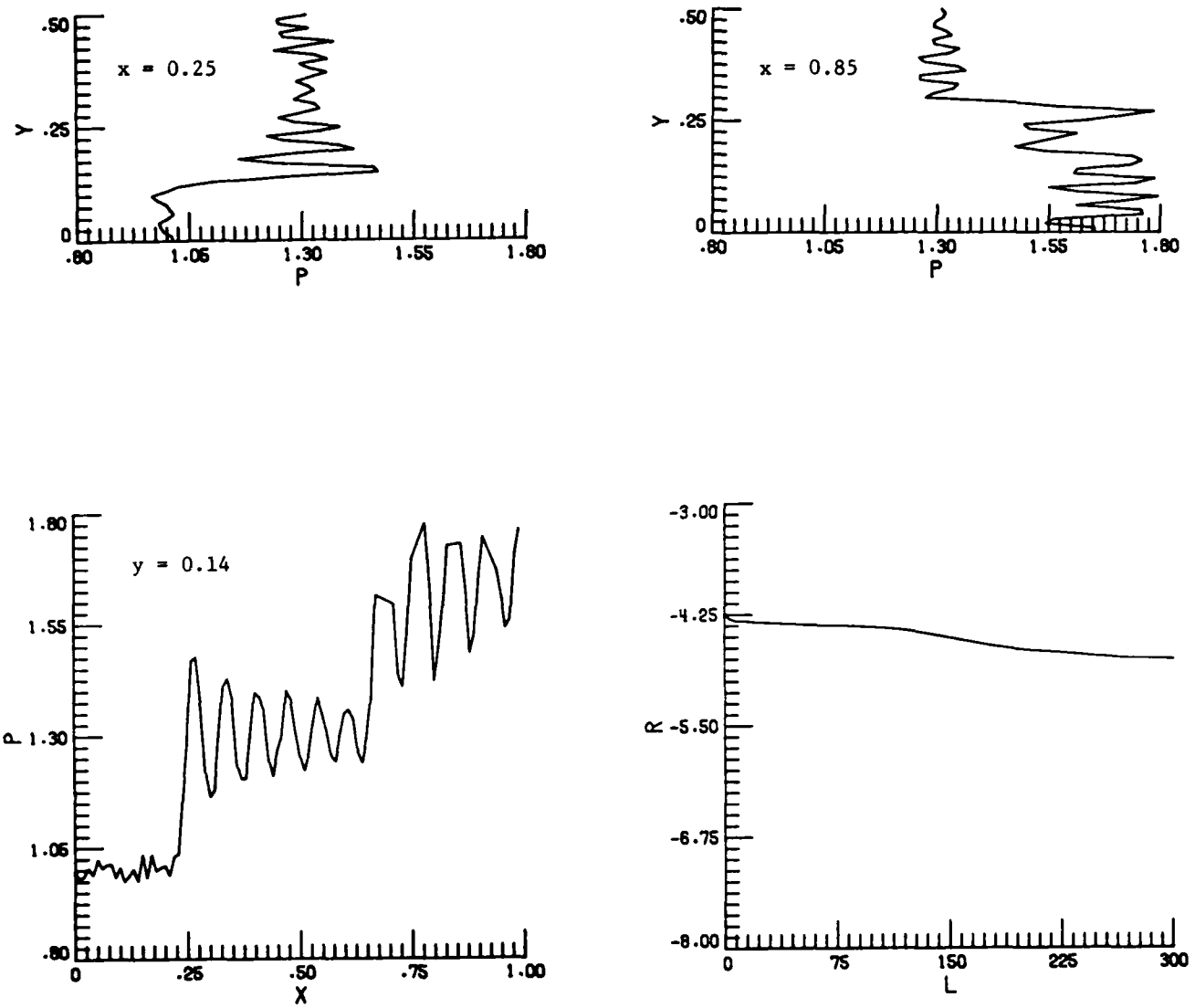

Figure 3a: Pressure distribution and residual plot for second order scheme ($\epsilon = 0, \kappa = 1.67$).

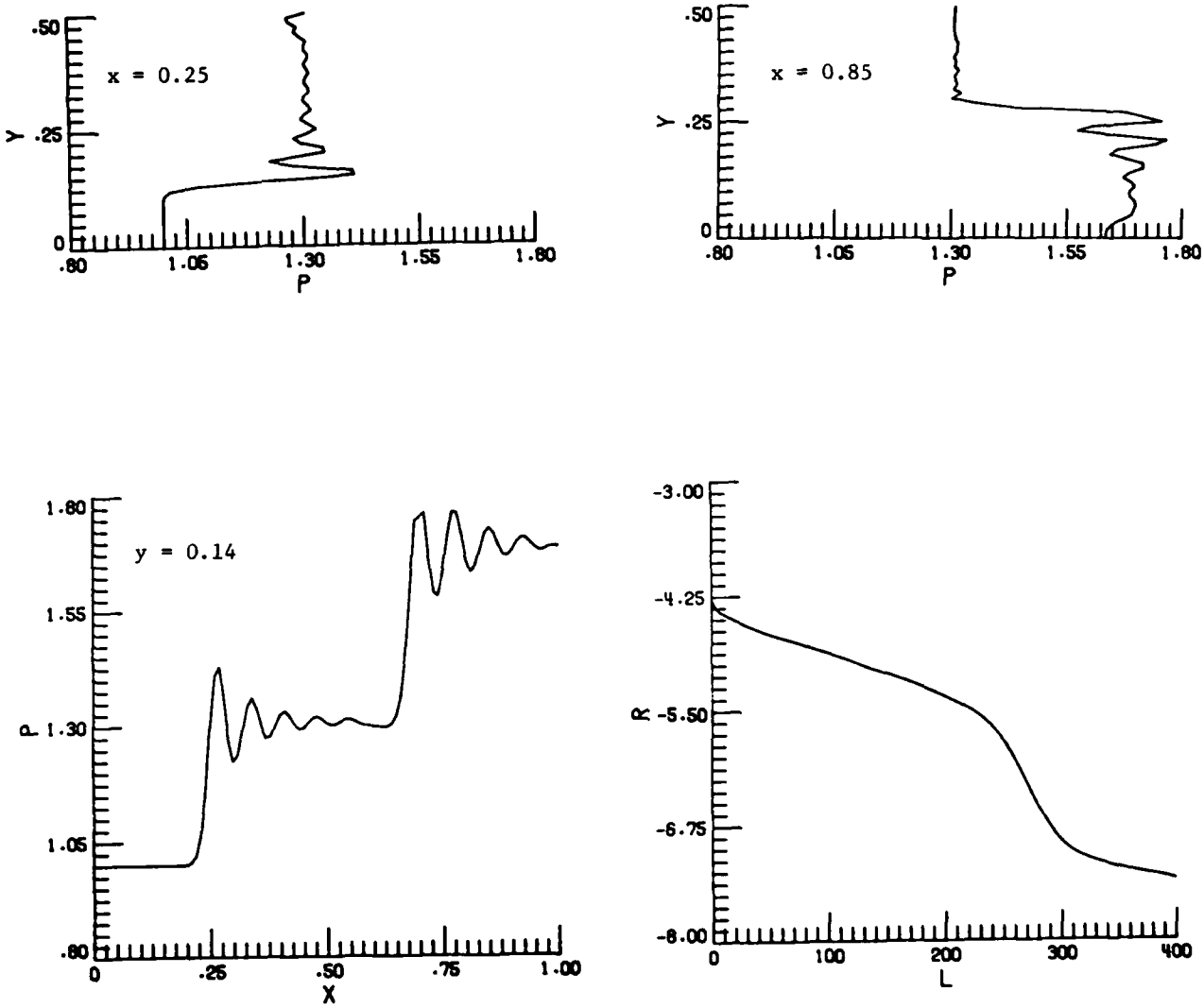

Figure 3b: Pressure distribution and residual plot for second order scheme ($\epsilon = 0.36, \kappa = 1.67$).

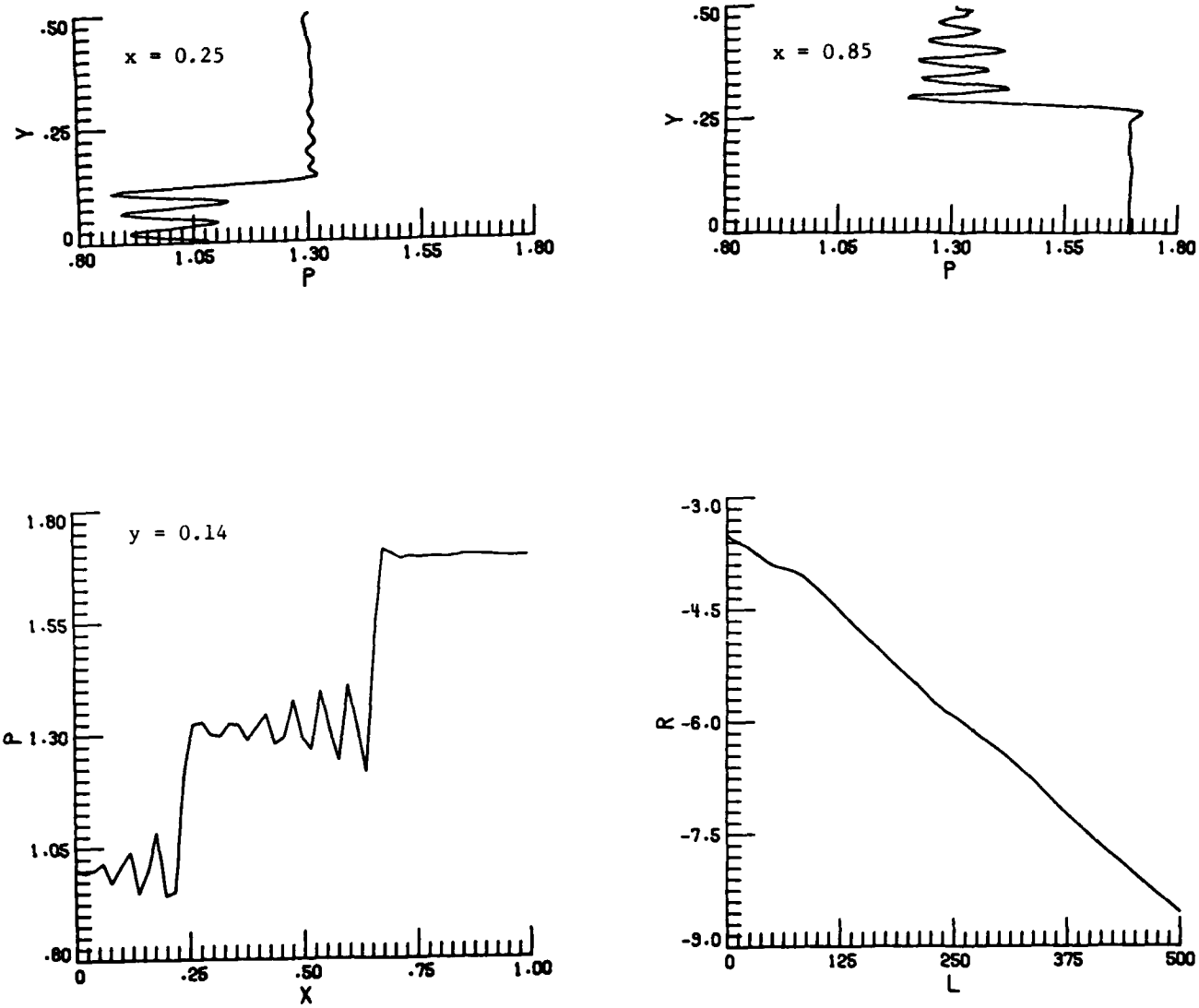

Figure 4: Pressure distribution and residual plot for compact scheme ($\epsilon = 0.36, \kappa = 1.01$).

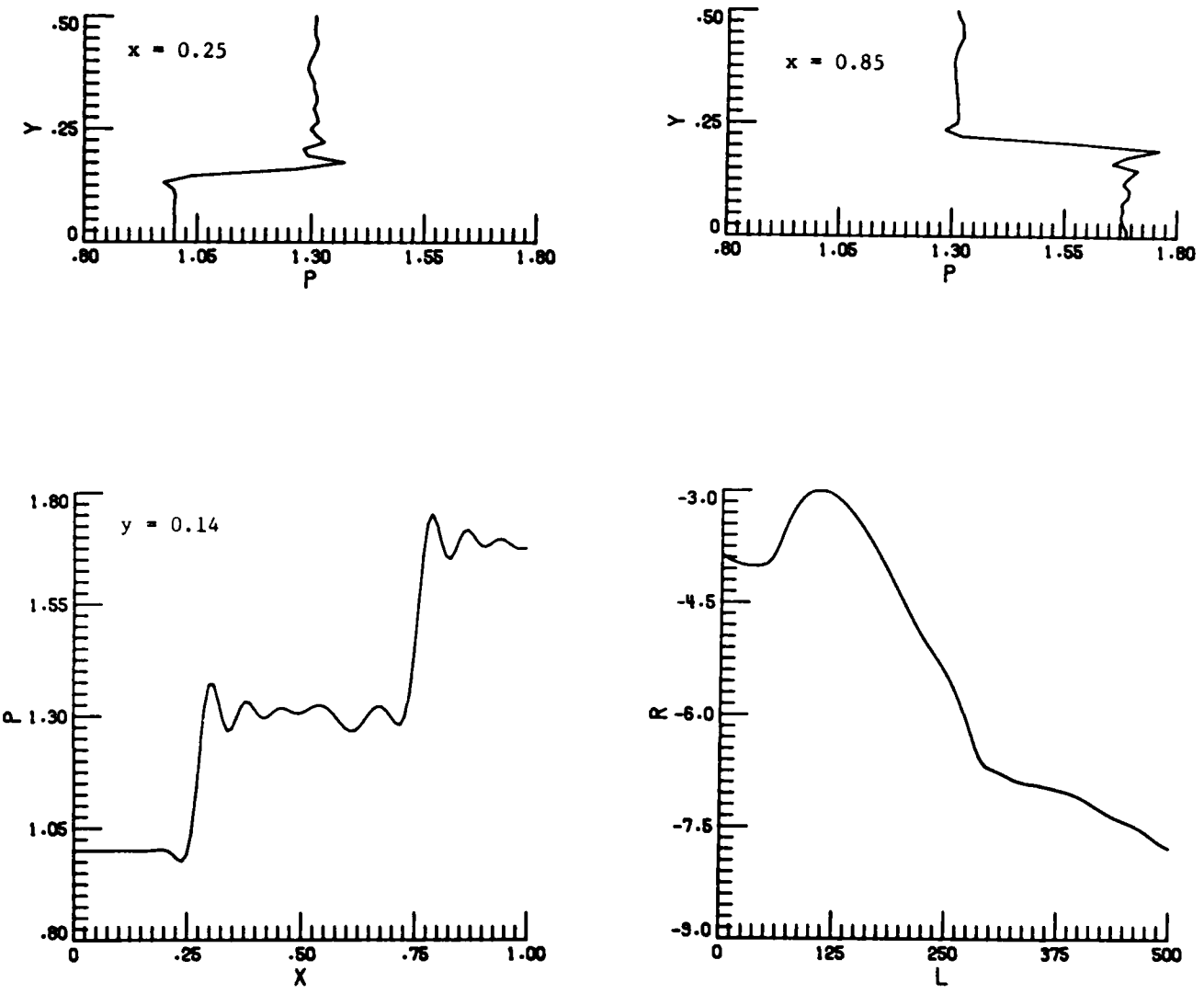

Figure 5: Pressure distribution and residual plot for compact scheme ($\epsilon = 0.36, \kappa = 0.42$).

END

DATE

FILMED

6-1988

DTIC